ACS Catalysis

Research Article

pubs.acs.org/acscatalysis

Intrinsic Ligand Effect Governing the Catalytic Activity of Pd Oxide Thin Films

Natalia M. Martin,*[,†] Maxime Van den Bossche,[‡] Anders Hellman,[‡] Henrik Grönbeck,[‡] Can Hakanoglu,[§] Johan Gustafson,[†] Sara Blomberg,[†] Niclas Johansson,[†] Zhi Liu,[∥] Stephanus Axnanda,[∥] Jason F. Weaver,[§] and Edvin Lundgren[†]

[†]Division of Synchrotron Radiation Research, Lund University, Box 118, SE-221 00 Lund, Sweden

[‡]Competence Centre for Catalysis and Department of Applied Physics, Chalmers University of Technology, SE-41296 Göteborg, Sweden

[§]Department of Chemical Engineering, University of Florida, Gainesville, Florida 32611, United States

[∥]Advanced Light Source, Lawrence Berkeley National Laboratory, Berkeley, California 94720, United States

ABSTRACT: High-pressure X-ray photoelectron spectroscopy, mass spectrometry, and density functional theory calculations have been combined to study methane oxidation over Pd(100). The measurements reveal a high activity when a two-layer PdO(101) oriented film is formed. Although a one-layer PdO(101) film exhibits a similar surface structure, no or very little activity is observed. The calculations show that the presence of an oxygen atom directly below the coordinatively unsaturated Pd atom in the two-layer PdO(101) film is crucial for efficient methane dissociation, demonstrating a ligand effect that may be broadly important in determining the catalytic properties of oxide thin films.

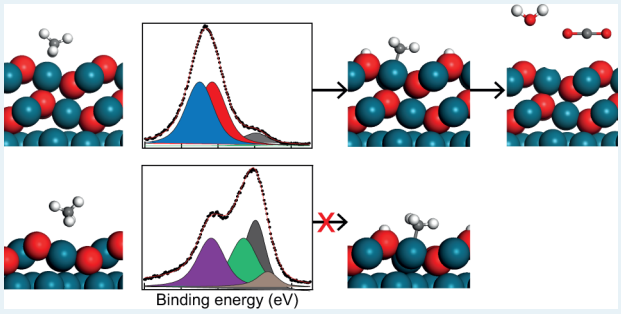

KEYWORDS: *heterogeneous catalysis, methane oxidation, palladium, PdO, ($\sqrt{5} \times \sqrt{5}$)*

INTRODUCTION

Catalytic techniques are crucial in modern society. They not only are used in the production of chemicals but also allow emission control and renewable energy solutions. Because of the vital importance and need for catalysts with enhanced performance, the nature of the active site during reaction conditions has been studied intensely.[1] It has, for example, been demonstrated that sites with undercoordinated atoms such as steps, kinks, and defects can dominate the reactivity of metal particles.[2] Similarly, coordinatively unsaturated (CUS) sites in oxides can play a crucial role in the measured catalytic activity.[3] Generally, one way to tune the reactivity of a given site is to modify its nearest neighbors. This, so-called, ligand effect has electronic origins and has within heterogeneous catalysis mainly been discussed in connection to metal alloys.[4] Far less is known about such effects in catalytically active thin oxide films, in particular under conditions close to reaction conditions.

Methane (CH_4) is the principal component of natural gas, and significant effort over the past several decades has been devoted to understanding the methane oxidation process.[5−12] In particular, Pd has been shown to be one of the most active catalysts for methane combustion in an excess of oxygen,[7,13−15] and it has been observed that variations in activity can be correlated to changes in the Pd oxidation state.[16,17] Recently, it was suggested that the high activity of palladium oxide for complete methane oxidation could be related to the presence of a particular PdO facet, namely PdO(101).[18] This is supported by ultrahigh vacuum (UHV) studies of the interaction of methane with the PdO(101) surface at low temperatures.[19−22]

Oxidation of Pd(100) is known to initially yield a surface oxide with a ($\sqrt{5} \times \sqrt{5}$) in-plane periodicity (hereafter denoted $\sqrt{5}$), which consists of a single PdO(101) monolayer adhered to the Pd(100) surface.[23−25] Further oxidation results in the epitaxial growth of several layers of bulklike PdO(101) exposing the stoichiometric (101) surface[26−28] to the gas phase. Both the $\sqrt{5}$ and the bulk PdO(101) have CUS Pd atoms at their surfaces. These are sites that potentially could be attractive for adsorption and dissociation of molecular species. However, there is a crucial difference between the two structures. Whereas each CUS Pd atom in the $\sqrt{5}$ structure is coordinated to two oxygen atoms (Figure 1b), each CUS Pd atom in the bulk PdO(101) surface is coordinated to three oxygen atoms, with the additional oxygen atom located directly below the CUS Pd atom (Figure 1a). Thus, the two systems offer the possibility of exploring ligand effects in oxidized palladium.

In this work, we show that the presence of the oxygen atom underneath the CUS Pd atom is essential for abstraction of the first hydrogen atom from the CH_4 molecule, which is thought

Received: July 16, 2014
Revised: August 18, 2014
Published: August 19, 2014

   dx.doi.org/10.1021/cs5010163 | ACS Catal. 2014, 4, 3330−3334

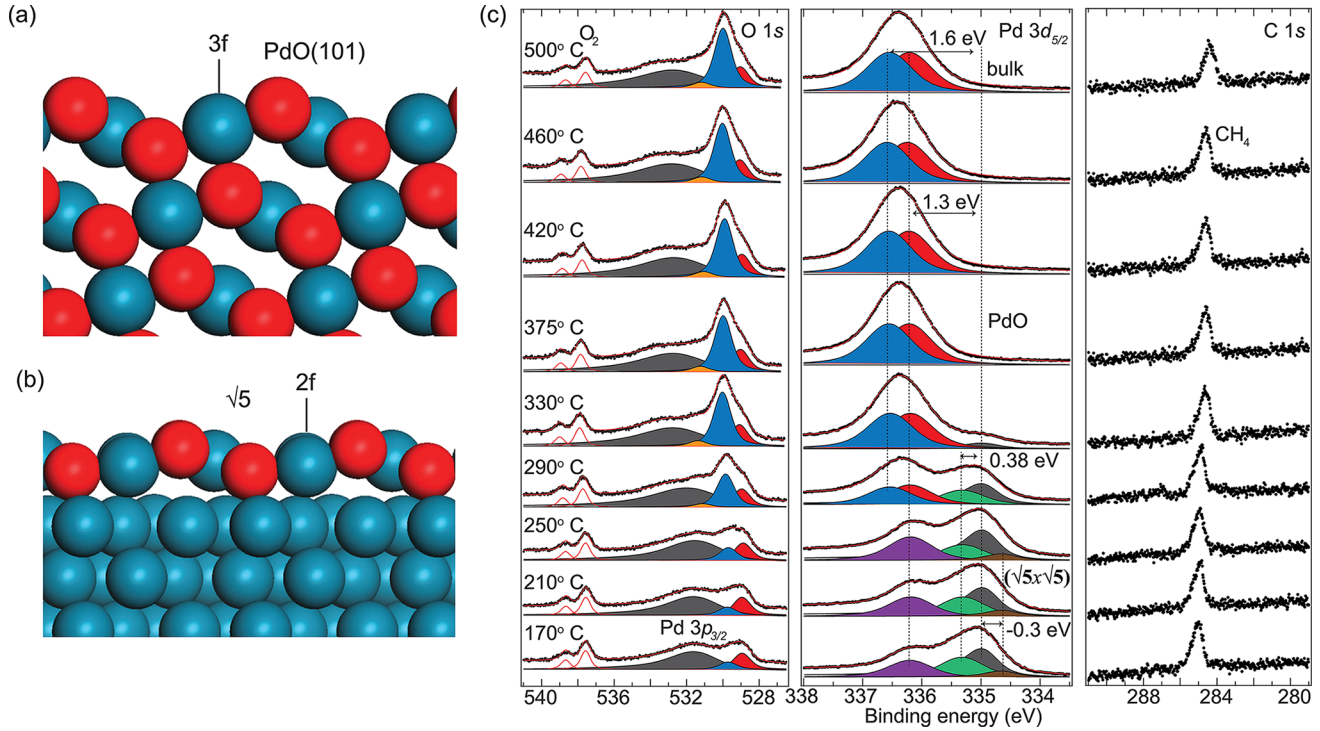

Figure 1. Side view of (a) the PdO(101) surface and (b) $\sqrt{5}$ surface. (c) O 1s, Pd $3d_{5/2}$, and C 1s core level spectra during methane oxidation in a gas mixture of 0.375 Torr of O_2 and 0.150 Torr of CH_4 as the sample temperature is increased.

to be the rate-determining step in the CH_4 oxidation process. The conclusion is based on high-pressure X-ray photoelectron spectroscopy (HP-XPS), mass spectrometry (MS), and density functional theory (DFT) calculations. The experiments suggest that no or very little CH_4 oxidation occurs on the $\sqrt{5}$ surface oxide, whereas high activity is observed for films thicker than one monolayer (ML). Complementary DFT calculations show that the oxygen atom below the CUS Pd atom in the PdO(101) surface reduces the Pauli repulsion between the CUS Pd atom and the CH_4 molecule, which allows for efficient methane dissociation. The results demonstrate a strong ligand effect in the surface chemistry of oxide thin films and underlines the critical importance of local geometry in heterogeneous catalysis.

EXPERIMENTAL AND COMPUTATIONAL METHODS

The HP-XPS measurements were performed at beamline 9.3.2 at the Advanced Light Source (ALS) in Berkeley, CA.[29,30] All spectra were collected in normal emission mode with photon energies of 435 eV for Pd $3d_{5/2}$ and C 1s and 650 eV for O 1s. The Pd(100) sample was mounted on a specially designed sample holder. The cleaning of the samples and the deconvolution of the spectra were identical to the procedures reported in ref 31. We found that the structure formed after exposing the Pd(100) sample to 0.0375 Torr of O_2 and 0.015 Torr of CH_4 at 150 °C gives rise to an XPS signature that resembles that obtained from the $\sqrt{5}$ surface oxide.[23] As a fully developed $\sqrt{5}$ surface oxide has a coverage of 0.8 ML of oxygen, the area underneath the O 1s oxide peak can be used to estimate the oxygen coverage. [1 ML equals the number of atoms on the Pd(100) surface.] The oxidation of methane to water and carbon dioxide was investigated at an O_2:CH_4 ratio of 5:2 and different total pressures of 0.525, 0.105, and 0.052 Torr.

DFT was applied with the gradient-corrected exchange-correlation functional according to Perdew, Burke, and Ernzerhof (PBE).[32] In particular, the plane-wave pseudopotential code VASP was used.[33−35] The kinetic energy cutoff for the basis set was set to 450 eV. Standard PAW potentials[36,37] were used to treat the interaction between the valence electrons and the core. Reciprocal space integration over the Brillouin zone was approximated with finite sampling using Monkhorst−Pack grids.[38,39] The $\sqrt{5}$ unit cell was sampled with 13 unique *k*-points. The system was modeled with five metal layers on which one or two PdO(101) monolayers are adhered. Successive slabs in the direction normal to the surface were separated by at least 12 Å. Gas phase methane was treated in a large cubic unit cell with a lattice constant of 12 Å. Geometry optimizations were conducted without any constraints, and the structures were considered relaxed when the largest force in the system was smaller than 0.01 eV/Å.

RESULTS AND DISCUSSION

Figure 1c shows the O 1s, Pd $3d_{5/2}$, and C 1s levels recorded during the CH_4 oxidation reaction in a mixture of 0.375 Torr of O_2 and 0.150 Torr of CH_4 while the temperature is increased from 170 to 500 °C in a stepwise manner. At low temperatures, the Pd $3d_{5/2}$ and O 1s levels exhibit the signature of the $\sqrt{5}$ surface oxide.[23] The O 1s level shows two components at 528.9 and 529.7 eV in addition to Pd $3p_{3/2}$ at 532 eV. Two components at 537.7 and 538.7 eV that correspond to gas phase O_2 are also observed.[40] In addition to the bulk peak, Pd $3d_{5/2}$ presents three components that are shifted by −0.3, +0.38, and +1.3 eV with respect to the bulk value. The O 1s components have previously been assigned[41] to the 3-fold (red) and 4-fold (blue) coordinated O atoms, whereas the Pd $3d_{5/2}$ components have been assigned to interface Pd atoms (brown) together with 2-fold (green) and 4-fold (violet) coordinated Pd

dx.doi.org/10.1021/cs5010163 | ACS Catal. 2014, 4, 3330−3334

atoms in the surface oxide. At the C 1s level, the CO_2 gas phase peak is too small to be detected because of the low reaction rate, but the peak from CH_4 is observed at ~285 eV.[42]

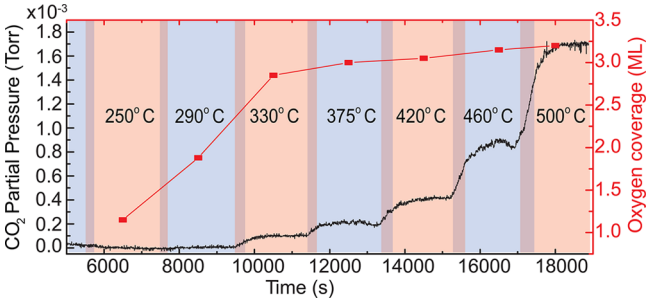

Figure 2. Rates of CO_2 production measured by mass spectrometry (left axis) and estimated oxygen coverage (right axis) as a function of time during CH_4 oxidation in 0.375 Torr of O_2 and 0.150 Torr of CH_4. The different temperatures are indicated in the shaded areas.

At 330 °C, the spectra resemble the signature of a thicker PdO(101) film.[28,41] The O 1s spectrum shows two components at 528.55 and 529.5 eV corresponding to the 3- and 4-fold coordinated O atoms, respectively, and the Pd $3d_{5/2}$ spectrum has two oxide components, shifted by 1.3 and 1.6 eV with respect to bulk Pd, corresponding to the 3- and 4-fold coordinated Pd atoms at the surface of PdO(101), respectively. The oxygen coverage at this temperature has increased to 2.85 ML. Furthermore, a new O 1s component (orange) appears above 290 °C at binding energies close to 531 eV. This feature corresponds to OH groups[41] and is consistent with methane dissociation. The magnitude of the OH component increases further at 330 °C, yielding under these conditions an OH coverage of ~24% with respect to the total number of 3-fold coordinated O atoms.

To estimate the CH_4 oxidation rate, Figure 2 shows the evolution of the CO_2 partial pressure as measured by MS, as well as the oxygen coverage as deduced from the HP-XPS measurements. A clear CO_2 signal is observed only at temperatures above 300 °C, which correspond to oxide thicknesses well above 1 ML. These results indicate a high activity when a film thicker than a single layer of PdO(101) has developed.

Similar measurements were performed at total pressures of 0.105 and 0.052 Torr, and the results from all three measurements are summarized in Figure 3. For all measurements, a CO_2 signal could be observed only at an oxygen coverage well above 1 ML and at temperatures above 330 °C, when a clear signature from multilayer PdO(101) could be observed in the XPS spectra. The oxygen coverages for each of the total pressures are indicated in Figure 3 (top panel). The corresponding Arrhenius plots for the methane oxidation over Pd(100) are reported in the bottom panel of Figure 3. We find activation energies of 0.74, 0.72, and 0.68 eV for the 0.052, 0.105, and 0.525 Torr experiments, respectively. The results are in good agreement with the activation energy for methane oxidation over crystalline PdO of 0.74−0.87 eV (17−20 kcal/mol)[9] and supported, oxidized Pd particles.[43]

DFT calculations were performed to investigate the marked difference in the ability to catalyze the methane oxidation reaction between one layer and several layers of PdO(101). As dissociation of methane into adsorbed methyl and hydrogen generally is assumed to be the rate-determining step,[18] we focus on this crucial step. Four different systems are investigated, namely, metallic Pd(100) [treated in a $p(2 \times 2)$ cell], one monolayer of PdO(101) supported on Pd(100) [$\sqrt{5}$−1 ML], two monolayers of PdO(101) supported on Pd(100) [$\sqrt{5}$−2 ML], and bulk PdO(101). The computed results for the adsorption energy, activation barrier, and reaction energy are listed in Table 1.

Methane is weakly adsorbed on all investigated surfaces. However, there is a clear difference between Pd(100) and $\sqrt{5}$−1 ML, where E_{ads} is close to zero as compared to the values for $\sqrt{5}$−2 ML and PdO(101) that have an adsorption well.[44] The measured adsorption energy of CH_4 on PdO(101) is reported to be −0.44 eV,[20] which is higher than the calculated

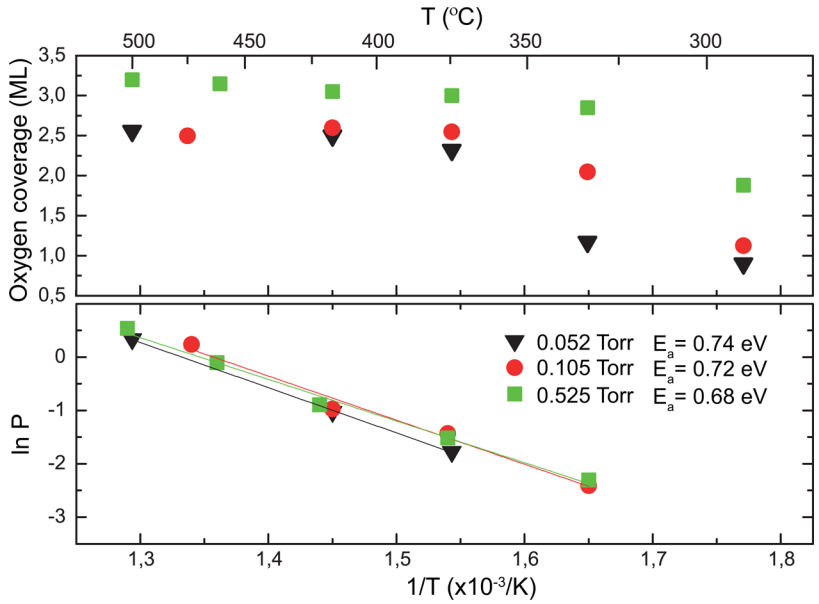

Figure 3. Oxygen coverage (top) as a function of inverse temperature for different total pressures during methane oxidation measurements over Pd(100) with a O_2:CH_4 ratio of 5:2. Corresponding Arrhenius plots (bottom) of the rate of formation of CO_2 over Pd(100).

dx.doi.org/10.1021/cs5010163 | ACS Catal. 2014, 4, 3330−3334

Table 1. Adsorption Energies (E_{ads}), Activation Barriers (ΔE), and Reaction Energies (E_r) As Calculated by DFT[a]

	Pd(100)	√5−1 ML	√5−2 ML	PdO(101)
E_{ads} (eV)	−0.03	−0.02	−0.14	−0.15
ΔE (eV)	0.77	1.34	0.66	0.68
E_r (eV)	0.40	0.40	−0.43	−0.39

[a]The reference energy for the activation barrier and the reaction energy is the bottom of the CH_4 adsorption well.

adsorption energy. The discrepancy is probably due to the lack of dispersion interactions in the applied exchange-correlation functional. A clear difference between the investigated surfaces is predicted in the activation barrier for methane dissociation. The barrier over √5−1 ML is 1.34 eV, whereas it is only 0.66 eV on √5−2 ML and similar for bulk PdO(101). This value is consistent with the experimentally determined apparent activation energy as presented in Figure 3 (0.68−0.74 eV). The dissociation is endothermic on Pd(100) and √5−1 ML, whereas it is exothermic on √5−2 ML and bulk PdO(101).

The calculated reaction properties of methane dissociation are in agreement with the results of our experiments. The √5 surface oxide is inactive, whereas 2 ML of PdO(101) supported on Pd(100) is thick enough to facilitate the reaction. To uncover the electronic reason for the differences in the activation energies, the potential energy curves for CH_4 approaching the √5−1 ML and √5−2 ML surfaces are reported in Figure 4. The two potential energy curves show a pronounced difference in how CH_4 interacts with the surfaces. The interaction with √5−1 ML is weak, and the Pauli repulsion between the molecule and the surface is significant at distances longer than 3 Å. In contrast, CH_4 experiences an adsorption well on √5−2 ML, and the Pauli repulsion becomes sizable only at distances shorter than ∼2.2 Å. The difference between the two surfaces implies that CH_4 is far from the final state (adsorbed methyl and hydrogen) when it dissociates on √5−1 ML whereas it is much closer on √5−2 ML. Thus, the potential energy surfaces for the initial and final states cross at a lower energy on √5−2 ML than on √5−1 ML. This is the reason for the low activation barrier.

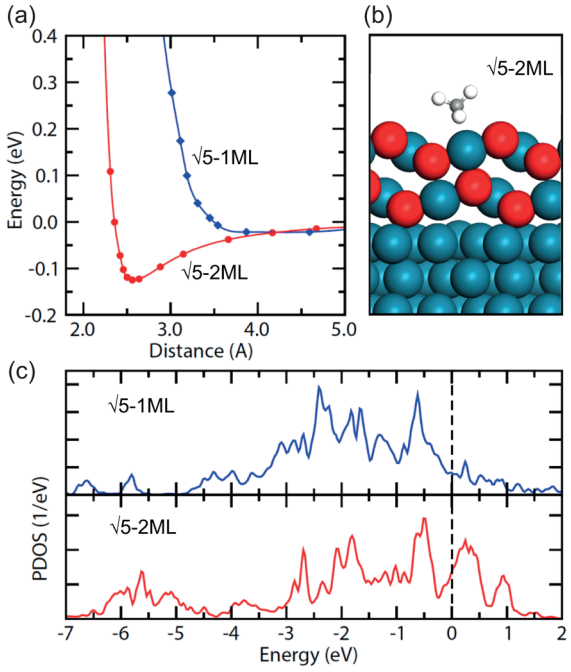

Figure 4. (a) Potential energy curves for CH_4 approaching √5−1 ML and √5−2 ML. (b) Structural model for CH_4 adsorbed on √5−2 ML (color codes as in Figure 1). (c) Partial density of states (PDOS) for √5−1 ML and √5−2 ML. The PDOS is given with respect to the Fermi energy.

To understand the electronic reason for the Pauli repulsion on √5−1 ML, the projected density of states (PDOS) is shown in Figure 4c. A similar effect has been reported previously for hydrogen[19] and CO[28] adsorption over PdO(101). The projection is done on the d_{z^2} atomic orbital on the Pd atom over which CH_4 dissociates. The d_{z^2} orbitals are the states that (if occupied) will cause a repulsion to the frontier methane orbital. There is a clear difference in the PDOS between the two surfaces. For √5−1 ML, most of the d_{z^2} states are below the Fermi energy, which means that they are occupied. In contrast, on √5−2 ML a part of the d_{z^2} states appear above the Fermi energy. It should be noted that d_{z^2} orbitals are hybridized with Pd 5s, which is a diffuse orbital. This explains the substantial repulsion experienced by CH_4 on √5−1 ML at long distances. The reason for the reduced level of occupation of d_{z^2} on the 3-fold coordinated Pd atoms in the √5−2 ML surface is the presence of an oxygen atom directly below the Pd atom. This is a ligand effect that is local and not connected to the development of the oxide character as the PdO film becomes thicker. To demonstrate this, we performed calculations for a free-standing PdO(101) monolayer. The energy of adsorption of CH_4 to the CUS site in the monolayer (only two oxygen neighbors) is zero and the barrier for dissociation 1.26 eV. If the CUS site in the free-standing film is coordinated to an electron-withdrawing ligand, methane is activated. Calculations were performed with chlorine (Cl) coordinated to the CUS site, and in this case, the adsorption energy of 2 ML PdO(101) is retained (E_{ads} = −0.14 eV) and the barrier for dissociation is reduced to 0.92 eV. These results show that it is possible to design sites for facile methane dissociation.

CONCLUSIONS

In summary, using a combination of HP-XPS, MS, and DFT calculations, we have demonstrated a ligand effect in thin Pd oxide structures for the activation of methane oxidation. We have shown that the efficiency of the reaction is strongly promoted by the presence of an oxygen atom directly underneath the CUS Pd atom in the PdO(101) structure. The role of the oxygen atom is to induce a reduction of the Pauli repulsion between the CUS Pd and the CH_4 molecule, which facilitates the abstraction of the first H atom from the molecule. The ligand effect in thin metal oxide films is likely to be present in other important catalytic material systems and may have broad implications for the atomistic design of catalysts.

AUTHOR INFORMATION

Corresponding Author

*E-mail: natalia.martin@sljus.lu.se.

Notes

The authors declare no competing financial interest.

dx.doi.org/10.1021/cs5010163 | ACS Catal. 2014, 4, 3330−3334

■ ACKNOWLEDGMENTS

The ALS staff is gratefully acknowledged. This work was financially supported by the foundation for strategic research (SSF), the Swedish Research Council, the Crafoord Foundation, the Knut and Alice Wallenberg Foundation, the Anna and Edwin Berger Foundation, COST Action CM1104, and NordForsk. The calculations were performed at C3SE (Göteborg, Sweden) and PDC (Stockholm, Sweden) via a SNIC grant. J.F.W. gratefully acknowledges financial support by the U.S. Department of Energy, Office of Basic Energy Sciences, Catalysis Science Division, through Grant DE-FG02-03ER15478. For the ALS measurements, we acknowledge the Director, Office of Science, Office of Basic Energy Sciences, of the U.S. Department of Energy under Contract DE-AC02-05CH11231.

■ REFERENCES

(1) Ertl, G., Knözinger, H., Weitkamp, J., Eds. *Handbook of Heterogeneous Catalysis*; Wiley-VCH Verlag GmbH: New York, 1997; Vol. *1*−*4*, pp 1−2123.
(2) Honkala, K.; Hellman, A.; Remediakis, I. N.; Logadottir, A.; Carlsson, A.; Dahl, S.; Christensen, C. H.; Nørskov, J. K. *Science* **2005**, *307*, 555−558.
(3) Over, H.; Kim, Y. D.; Seitsonen, A. P.; Wendt, S.; Lundgren, E.; Schmid, M.; Varga, P.; Morgante, A.; Ertl, G. *Science* **2000**, *287*, 1474−1476.
(4) Gauthier, Y.; Schmid, M.; Padovani, S.; Lundgren, E.; Bus, V.; Kresse, G.; Redinger, J.; Varga, P. *Phys. Rev. Lett.* **2001**, *87*, 0361031.
(5) Cullis, C. F.; Willat, B. M. *J. Catal.* **1983**, *83*, 267−285.
(6) Briot, P.; Primet, M. *Appl. Catal.* **1991**, *68*, 301−314.
(7) Burch, R.; Urbano, F. J. *Appl. Catal., A* **1995**, *124*, 121−138.
(8) Aryafar, M.; Zaera, F. *Catal. Lett.* **1997**, *48*, 173−183.
(9) Ciuparu, D.; Lyubovsky, M. R.; Altman, E.; Pfefferle, L. D.; Datye, A. *Catal. Rev.* **2002**, *44*, 593−649.
(10) Gélin, P.; Primet, M. *Appl. Catal., B* **2002**, *39*, 1−37.
(11) Li, Z.; Hoflund, G. N. *J. Nat. Gas Chem.* **2003**, *12*, 153−160.
(12) Inderwildi, O.; Jenkins, S. J. *Chem. Soc. Rev.* **2008**, *37*, 2274−2309.
(13) Farrauto, R. J.; Lampert, J. K.; Hobson, M. C.; Waterman, E. M. *Appl. Catal., B* **1995**, *6*, 263−270.
(14) Salomonsson, P.; Johansson, S.; Kasemo, B. *Catal. Lett.* **1995**, *33*, 1−13.
(15) Burch, R.; Loader, P.; Urbano, F. *Catal. Today* **1996**, *47*, 243−248.
(16) Monteiro, R. S.; Zemlyanov, D.; Storey, J. M.; Ribeiro, F. H. *J. Catal.* **2001**, *199*, 291−301.
(17) Gabasch, H.; Hayek, K.; Klötzer, B.; Unterberger, W.; Kleimenov, E.; Teschner, D.; Zafeiratos, S.; Hävecker, M.; Knop-Gericke, A.; Schlögl, R.; Aszalos-Kiss, B.; Zemlyanov, D. *J. Phys. Chem. C* **2007**, *111*, 7957−7962.
(18) Hellman, A.; Resta, A.; Martin, N. M.; Gustafson, J.; Trinchero, A.; Carlsson, P.-A.; Balmes, O.; Felici, R.; Van Rijn, R.; Frenken, J. W. M.; Andersen, J. N.; Lundgren, E.; Grönbeck, H. *J. Phys. Chem. Lett.* **2012**, *3*, 678−682.
(19) Blanco-Rey, M.; Wales, D. J.; Jenkins, S. J. *J. Phys. Chem. C* **2009**, *113*, 16757−16765.
(20) Weaver, J. F.; Hakanoglu, C.; Hawkins, J. M.; Asthagiri, A. *J. Chem. Phys.* **2010**, *132*, 0247091.
(21) Weaver, J. F.; Hinojosa, J. A., Jr.; Hakanoglu, C.; Antony, A.; Hawkins, J. M.; Asthagiri, A. *Catal. Today* **2011**, *160*, 213−227.
(22) Weaver, J. F. *Chem. Rev.* **2013**, *113*, 4164−4215.
(23) Todorova, M.; Lundgren, E.; Blum, V.; Mikkelsen, A.; Gray, S.; Gustafson, J.; Borg, M.; Rogal, J.; Reuter, K.; Andersen, J. N.; Scheffler, M. *Surf. Sci.* **2003**, *541*, 101−112.
(24) Kostelnik, P.; Seriani, N.; Kresse, G.; Mikkelsen, A.; Lundgren, E.; Blum, V.; Sikola, T.; Varga, P.; Schmid, M. *Surf. Sci.* **2007**, *601*, 1574−1581.
(25) Gustafson, J.; Shipilin, M.; Zhang, C.; Stierle, A.; Hejral, U.; Ruett, U.; Gutowski, O.; Carlsson, P.-A.; Skoglundh, M.; Lundgren, E. *Science* **2014**, *343*, 758−761.
(26) Seriani, N.; Harl, J.; Mittendorfer, F.; Kresse, G. *J. Chem. Phys.* **2009**, *131*, 0547011.
(27) Van Rijn, R.; Balmes, O.; Resta, A.; Wermeille, D.; Westerström, R.; Gustafson, J.; Felici, R.; Lundgren, E.; Frenken, J. W. *Phys. Chem. Chem. Phys.* **2011**, *13*, 13167−13171.
(28) Westerström, R.; Messing, M. E.; Blomberg, S.; Hellman, A.; Grönbeck, H.; Gustafson, J.; Martin, N. M.; Balmes, O.; Van Rijn, R.; Andersen, J. N.; Deppert, K.; Bluhm, H.; Liu, Z.; Grass, M. E.; Hävecker, M.; Lundgren, E. *Phys. Rev. B* **2011**, *83*, 1154401.
(29) Grass, M. E.; Karlsson, P. G.; Aksoy, F.; Lundqvist, M.; Wannberg, B.; Mun, B. S.; Hussain, Z.; Liu, Z. *Rev. Sci. Instrum.* **2010**, *81*, 0531061.
(30) Chang, R.; Hong, Y. P.; Axnanda, S.; Mao, B.; Jabeen, N.; Wang, S.; Tai, R.; Liu, Z. *Curr. Appl. Phys.* **2012**, *12*, 1292−1296.
(31) Blomberg, S.; Hoffmann, M. J.; Gustafson, J.; Martin, N. M.; Fernandes, V. R.; Borg, A.; Liu, Z.; Chang, R.; Matera, S.; Reuter, K.; Lundgren, E. *Phys. Rev. Lett.* **2013**, *110*, 1176011.
(32) Perdew, J. P.; Burke, K.; Ernzerhof, M. *Phys. Rev. Lett.* **1996**, *77*, 3865−3868.
(33) Kresse, G.; Hafner, J. *Phys. Rev. B* **1994**, *49*, 14251−14271.
(34) Kresse, G.; Furthmüller, J. *Comput. Mater. Sci.* **1996**, *6*, 15−50.
(35) Kresse, G.; Furthmüller, J. *Phys. Rev. B* **1996**, *54*, 11169−11186.
(36) Blöchl, P. E. *Phys. Rev. B* **1994**, *50*, 17953−17979.
(37) Kresse, G.; Joubert, D. *Phys. Rev. B* **1999**, *59*, 1758−1775.
(38) Monkhorst, H. J.; Pack, J. D. *Phys. Rev. B* **1976**, *13*, 5188−5192.
(39) Pack, J. D.; Monkhorst, H. J. *Phys. Rev. B* **1977**, *16*, 1748−1749.
(40) Hedman, J.; Heden, P.-F.; Nordling, C.; Siegbahn, K. *Phys. Lett. A* **1969**, *29*, 178−179.
(41) Martin, N. M.; Van den Bossche, M.; Grönbeck, H.; Hakanoglu, C.; Gustafson, J.; Blomberg, S.; Arman, A.; Antony, A.; Rai, R.; Asthagiri, A.; Weaver, J. F.; Lundgren, E. *J. Phys. Chem. C* **2013**, *117*, 13510−13519.
(42) Siegbahn, K.; Nordling, C.; Johansson, G.; Hedman, J.; Heden, P. O.; Hamrin, K.; Gelius, U.; Bergmark, T.; Werme, L. O.; Manne, R.; Bear, Y. *ESCA Applied to Free Molecules*; North-Holland Publishing Co.: Amsterdam, 1969.
(43) Chin, Y. H.; Buda, C.; Neurock, M.; Iglesia, E. *J. Am. Chem. Soc.* **2013**, *135*, 15425−15442.
(44) We note that the present implementation of DFT does not account for van der Waals interactions, which are imporant for an accurate description of methane in the physisorbed state; however, the governing mechanism for facile dissociation is based on a reduced Pauli repulsion, which is a strong interaction. Moreover, as the adsorption energy is low, adsorbed methane is not present on the surface under reaction conditions. However, we have investigated the initial and final states on PdO(101) using vdW-DF1 (Dion, M.; Rydberg, H.; Schroder, E.; Langreth, D. C.; Lundqvist, B. I. *Phys. Rev. Lett.* **2004**, *92*, 246401.) and vdW-DF2 (Lee, K.; Murray, D. E.; Kong, L.; Lundqvist, B. I.; Langreth, D. C. *Phys. Rev. B* **2010**, *82*, 081101). The adsorption energy of (CH_4) is −0.14, −0.15, and −0.20 eV within PBE, vdW-DF1, and vdW-DF2, respectively. The adsorption energy of (CH_3+H) is −0.55, −0.49, and −0.48 eV within PBE, vdW-DF1, and vdW-DF2, respectively. Thus, inclusion of van der Waals interactions with these functionals gives results similar to those of PBE.